Rydberg-atom masers. II. Triggering by external radiation and application to millimeter-wave detectors

P. Goy, L. Moi,* M. Gross, J. M. Raimond, C. Fabre, and S. Haroche
Laboratoire de Physique de l'Ecole Normale Superieure,
24 rue Lhomond, 75231 Paris Cedex 05, France
(Received 16 March 1982)

The "triggering" of transient maser systems using excited Rydberg atoms as active medium is investigated theoretically and experimentally. We show how the maser pulse characteristics are modified by the interaction of the active medium with small amounts of resonant mm-wave radiation. The phase, polarization, and emission delay of the radiated field are modified by this triggering: this can be used to detect very small powers of mm- or sub-mm-wave radiation. A complete discussion of the quantum and thermal noise of these detectors is presented. A demonstration of the feasibility of this technique is reported. Triggering signals corresponding to a detectivity of 3×10^{-17} W/Hz$^{1/2}$ at 108 GHz ($\lambda=2.8$ mm) have been measured at room temperature. The quantum-noise limit—corresponding to 6×10^{-19} W/Hz$^{1/2}$—should be reached with liquid-helium-temperature-cooled detectors.

I. INTRODUCTION

In a preceding paper,[1] hereafter referred to as RAM I, we have presented a simple theoretical description of transient Rydberg atom masers operating in the millimeter (mm)-wave domain and described some experiments performed with these devices. In this second paper, we focus on the "triggering" of these maser systems by external radiation impinging on the atomic medium and we study, theoretically and experimentally, various applications of this effect to the detection of millimeter-wave radiation.

Transient Rydberg masers are, as other similar super-radiant devices, unstable systems whose emission is initiated by electromagnetic field fluctuations. At 0 K background temperature, these fluctuations are due to spontaneous emission and the transient regime of Rydberg masers starts on the vacuum field fluctuations noise. At a finite background temperature T, the fluctuations of thermal radiation add their effect and, as soon as $k_BT/\hbar\omega \gtrsim 1$, overcome the vacuum field ones (k_B and $\hbar$: Boltzmann and Planck constants; ω: maser frequency). The maser emission is then initiated by the blackbody background photons present in the cavity. In RAM I, we have merely recalled the *ad hoc* semiclassical procedure used to describe the effect of the vacuum field fluctuations on the atomic system and we have generalized it, without demonstration, to introduce the effects of blackbody radiation as well. At 0 K, the procedure amounts to assigning an initial random polarization to the atoms in the maser cavity. The amplitude of this polarization obeys a Gaussian statistics with a mean value inversely proportional to the square root of the atom number N_0. The random choice of the initial polarization governs the delay of the maser emission bursts which slightly fluctuates from one realization of the experiment to the next. In order to describe the maser initiation for $T\neq0$ K, we have in RAM I assumed, without proof, that the initial polarization still obeys Gaussian statistics with a new mean value which is now proportional to $[(1+\bar{n}_B)/N_0]^{1/2}$, where $\bar{n}_B=[\exp(\hbar\omega/k_BT)-1]^{-1}$ is the average number of blackbody photons per cavity mode ($\bar{n}_B\simeq k_BT/\hbar\omega$ in the Rayleigh-Jeans limit, $k_BT\gg\hbar\omega$). This change in the initial condition entails a logarithmic change in the delay of the maser emission. More generally it is clear that any external electromagnetic field impinging on the atoms, whether it is of thermal origin or not, will induce measurable changes in the maser emission behavior, since it will perturb the early stage of the radiation process which largely governs the bulk of the emission characteristics.

In this paper, we propose to study these changes theoretically and experimentally. In a first theoretical part (Sec. II) we will essentially solve the following simple problem. We will assume that a small external electromagnetic field with well-defined frequency, phase, and polarization impinges on the

maser active medium at the very moment when its initial population inversion is achieved and we will study all the modifications of the maser emission characteristics induced by this signal. The interest in this problem is twofold: (i) Once the response of the maser system to triggering by monochromatic radiation is known, it is only a matter of amplitude and phase averaging to compute the effect of random field triggering. We will thus be able to derive the maser response to blackbody radiation and give solid ground to the formulas quoted without proof in RAM I; (ii) as we will see, the modifications to emission induced by an external perturbation are very sensitive to the amplitude of this perturbation. Not only the delay of the emission is (logarithmically) changed, but also the polarization and phase fluctuations of the emitted field are drastically modified. The maser emission tends to lock on the polarization and phase of the impinging signal as soon as it becomes of the order of the spontaneous (or blackbody) fluctuations. As a result, one can make use of these changes to detect very small amounts of millimeter-wave radiation and thus achieve detectors whose sensitivity is basically limited by the background temperature, a very attractive possibility in a frequency domain (100 to 300 GHz and more) where good detectors are in high demand. In the experimental part of this paper (Secs. III and IV), we describe experiments in which we have demonstrated the practical feasibility of such unstable triggered detectors, very similar in their principle to recently reported triggered superradiant devices operating in the near-infrared domain.[2,3] We will show that signals of the order of blackbody radiation noise at room temperature are detected with a present detectivity figure of 3.10^{-17} $W/Hz^{1/2}$. This is a clear indication that Rydberg masers could be used at low temperature as quantum (single photon) detectors of millimeter-wave radiation.

The setup used to perform these experiments is basically the same as the one described in RAM I, with a major difference concerning the detection procedure. Instead of detecting indirectly the maser emission through Rydberg level population changes, we observe directly the bursts of millimeter-wave radiation with the help of a heterodyne Schottky diode receiver. This technique provides us with the time resolution and the phase and polarization sensitivities which were lacking in the indirect method and which are clearly essential features in these triggering experiments. Section III of this paper is devoted to the detailed analysis of this new detection method along with the description of the millimeter-wave calibrated source used to trigger the maser emission. In Sec. IV, the triggering experiments themselves are described and a detailed analysis of the sensitivity of the technique is presented. Obviously, the present stage of this experiment is only preliminary to a more complete study of the possibility of these new devices. Improvements, presently in progress in our laboratory, include the cooling of the whole system to liquid-helium temperature in order to reduce the blackbody background noise. These improvements will be rapidly discussed in the last concluding part (Sec. V).

II. THEORY OF RYDBERG MASER TRIGGERING

We are interested here in the description of the evolution of an ensemble of Rydberg atoms placed in an open Fabry-Perot cavity, prepared at time $t=0$ in a given initial state and subjected to the effect of a continuous-wave small external electromagnetic field. We choose to describe the system evolution within the semiclassical framework already outlined in RAM I. The atomic polarization $\mathscr{P}(z,t)$, the population inversion $\mathscr{N}(z,t)$, and the field envelope $\mathscr{E}(z,t)$ evolve according to coupled nonlinear Bloch-Maxwell equations. We restrict ourselves to the case of a moderate finesse cavity. In the absence of triggering, we have seen in RAM I that the emission consists in a single burst of radiation emitted after a delay of a few T_R (T_R being a characteristic maser evolution time inversely proportional to the atom number N_0). It is clear that the effect of a small injected field on this system is important only at the beginning of the emission process, when the self-radiated component is still small. After a time of the order of T_R, the self-radiated component starts to dominate the small impinging field and the effect of the latter one on the system evolution rate becomes indeed quite negligible. In other words, it is important to study the modification induced by the impinging field only during the early phase ($0<t\lesssim T_R$) of the emission process and one can disregard its contribution during the bulk of the emission. What happens in the early phase of the process is however very important, inasmuch as it governs several features of the emission at later stages. As we have seen in RAM I, the delay of the emission, its fluctuations, and the emitted field polarization all depend on what has taken place during the crucial time around

$t=0$. These simple considerations naturally lead us to solve the problem in the following way. The system evolution is divided into two stages: an early evolution phase (invisible for the detectors since the field is too small) during which the injected triggering field is taken into account ($0<t\lesssim$ a few T_R) and a latter ($t>$ a few T_R) phase during which the main (i.e., measurable part) of the evolution does occur and during which one can consider that the triggering field has been switched off. A very simple approximation can be made for the study of the first stage. It is legitimate to assume that the population inversion has not appreciably changed from its initial value, which amounts to replacing in the Bloch-Maxwell equations the time-varying $\mathcal{N}(z,t)$ quantities by the constant N_0. The equations then become linear, which considerably simplifies their solution. The atomic polarization appears to be the sum of two independent exponentially increasing contributions: a "spontaneous" one, which is the one that one would obtain for a free-running, untriggered maser and an induced one, which is proportional to the triggering signal. The ratio of these two solutions is a measure of the triggering effect. This linear solution, valid up to time $t\sim T_R$, can then be considered as a new initial condition imposed to the evolution of the maser in the later phase. This phase obeys more complicated nonlinear equations but, on the other hand, the effect of the injected field can be neglected during it and the general form of the solution is known from the free maser problem. One then essentially has to understand how the change in the initial condition of the nonlinear problem does modify the feature of the emission process. In fact, the whole procedure we have just outlined is a mere generalization to the case of triggering by an external field of the one which is used to describe the initiation of super radiance by the spontaneous emission field.[4-6] One can indeed consider that the maser is triggered by two competing fields: the vacuum fluctuation field and the impinging one, and it is quite natural to use the same theoretical method to describe the effects of both perturbations.

We start this section by recalling the notations and the results of RAM I concerning the case of a free-running maser triggered by spontaneous emission only (Sec. II A). We then briefly introduce the linearized Bloch-Maxwell equations which describe the early stage of the maser emission in the presence of a small monochromatic triggering signal (Sec. II B). We solve these equations and we compare the spontaneous and "triggered" contributions by defining a triggering factor η that we simply express in terms of the number of triggering photons impinging in the maser cavity during the characteristic time T_R (Sec. II C). We next show how the emission delays and phase depend upon this triggering factor (Sec. II D). The effect on the field polarization are discussed in Sec. II E. Application of the formalism to the case of triggering by blackbody radiation is presented in Sec. II F where we demonstrate the formulas admitted in RAM I. Section II G deals with the practically important case in which the maser is triggered by blackbody photons *and* by an additional external signal. The analysis of this case allows us to evaluate the thermal noise of a detector based on the maser triggering effect, which will be essential for the discussion of the experiments described in Sec. IV.

A. "Free-running" maser equations

For sake of completeness, we recall in this subsection the main results of RAM I concerning the evolution of an untriggered "free-running" Rydberg atom maser. We are dealing as in RAM I with a maser made of N_0 two-level atoms in an open Fabry-Perot cavity (in fact, the actual atoms are emitting on an $nS_{1/2}\rightarrow n'P_{1/2}$ transition between two levels exhibiting each a twofold degeneracy. As shown in RAM I and as discussed below in Sec. II E, this situation can be analyzed in terms of a superposition of two classes of two-level atoms). For sake of simplicity, we restrict ourselves to the case of an active medium much smaller than the emission wavelength λ. In that case all atoms see the same electromagnetic field $\mathcal{E}_0(t)$ and they all have the same polarization $\mathcal{P}(t)$ and population difference $\mathcal{N}(t)$ between the upper and the lower state. When no impinging radiation falls on the system (free-running or spontaneous maser), $\mathcal{P}(t)$, $\mathcal{N}(t)$, and $\mathcal{E}_0(t)$ obey the following Bloch-Maxwell equations [Eqs. (8) and (11) in RAM I]:

$$\frac{d\mathcal{P}}{dt}=\frac{id^2}{\hbar}\mathcal{E}_0\mathcal{N}\,, \tag{1a}$$

$$\frac{d\mathcal{N}}{dt}=\frac{i}{2\hbar}(\mathcal{E}_0^*\mathcal{P}-\mathcal{E}_0\mathcal{P}^*)\,, \tag{1b}$$

$$\frac{d\mathcal{E}_0}{dt}=-\frac{\mathcal{E}_0}{2T_{\rm cav}}-\frac{2i\omega}{\epsilon_0\pi w_0^2 L}\mathcal{P}\,, \tag{1c}$$

where d is the electric dipole matrix element between the two states involved in the transition (typically 500 a.u. for a transition between neighbor

Rydberg levels with principal quantum number $n \sim 30$), ω is the atomic frequency, and $T_{\rm cav}$, w_0, and L are the cavity damping time, transverse waist dimension, and intermirror length, respectively. The solution of Eqs. (1a)–(1c) is readily obtained by the introduction of the Bloch angles θ_0 and ϕ defined by

$$\mathcal{N}=N_0\cos\theta_0 , \tag{2a}$$

$$\mathcal{P}=iN_0 d\sin\theta_0 e^{i\phi} , \tag{2b}$$

which in the case of a short-damping time cavity (see condition below) obey the following equations:

$$\frac{d\phi}{dt}=0 , \tag{3a}$$

$$\frac{d\theta_0}{dt}=\frac{1}{2T_R}\sin\theta . \tag{3b}$$

T_R is the characteristic maser emission time defined as

$$T_R^{-1}=\frac{8}{\pi}f\Gamma N_0\mu , \tag{4}$$

where f is the cavity finesse, related to $T_{\rm cav}$ and L by the relation

$$T_{\rm cav}=\frac{1}{\pi}f\frac{L}{c} . \tag{5}$$

Γ is the partial spontaneous emission rate associated to the transition

$$\Gamma=\frac{\omega^3 d^2}{3\pi\epsilon_0\hbar c^3} \tag{6}$$

and μ is proportional to the diffraction limited solid angle of the cavity mode:

$$\mu=\frac{3}{4\pi^2}\frac{\lambda^2}{w_0^2} . \tag{7}$$

The condition for Eq. (3b) validity is that T_R should be much longer than $T_{\rm cav}$:

$$T_R \gg T_{\rm cav} . \tag{8}$$

Knowing $\theta(t)$ from the solution of Eq. (3b), the field envelope $\mathcal{E}_0(t)$ is given by

$$e^{i\phi}\frac{d\theta_0}{dt}=\frac{\mathcal{E}_0(t)d}{\hbar} . \tag{9}$$

The initial value θ_0^i and ϕ^i of θ_0 and ϕ at time $t=0$ are, for a free-running maser, random quantities reflecting the fluctuations of the vacuum field. The probability laws for θ_0^i and ϕ^i are

$$P(\phi^i)=\frac{1}{2\pi} , \tag{10a}$$

$$P(\theta_0^i)=\frac{2\theta_0^i}{\bar{\theta}^2}\exp\left[-\left[\frac{\theta_0^i}{\bar{\theta}^2}\right]^2\right] \tag{10b}$$

with a mean-square value $\bar{\theta}$ for θ_0^i given by

$$\bar{\theta}=2N_0^{-1/2} . \tag{11}$$

Starting from the small nonzero θ_0^i value, θ_0 evolves according to the damped-pendulumlike equation (3b) and reaches the value $\theta_0=\pi$ at time $t=+\infty$. The light intensity proportional to $(d\theta_0/dt)^2$ exhibits a bell-shaped time variation described by the hyperbolic secant solution

$$\left[\frac{d\theta_0}{dt}\right]^2=\frac{1}{4T_R^2}\frac{1}{\cosh^2[(t-t_D)/2T_R]} \tag{12}$$

whose delay t_D fluctuates from one realization of the experiment to the next, reflecting the distribution of possible θ_0^i values. The delay $t_D(\theta_0^i)$ corresponding to an initial value θ_0^i is

$$t_d(\theta_0^i)=-2T_R\ln\left[\frac{\theta_0^i}{2}\right] . \tag{13a}$$

The average delay $\langle t_D\rangle$ and delay fluctuation

$$\Delta t_D=(\langle t_D^2\rangle-\langle t_D\rangle^2)^{1/2}$$

are given by

$$\langle t_D\rangle=T_R\ln N_0 , \tag{13b}$$

$$\Delta t_D=1.3T_R . \tag{13c}$$

B. Triggered maser evolution in the linear regime

Let us now assume that a small electromagnetic field radiated by an external source impinges on the active medium (it is coupled to the cavity through a waveguide). Let us call $\mathcal{E}_t$ the complex amplitude of the impinging radiation at the atom location in the cavity. This field is monchromatic with a frequency which, for sake of generality, is assumed to be detuned by a small amount $\Delta\omega$ from the transition frequency ω. $\Delta\omega$, which might be of the order of or larger than the maser bandwidth T_R^{-1}, is assumed to be much smaller than the cavity width $T_{\rm cav}^{-1}$, so that the cavity can sustain the triggering field:

$$\Delta\omega T_{\rm cav} \ll 1 . \tag{14}$$

With these assumptions, the Maxwell equation (1c) of the free-running maser has to be modified and now reads

$$\frac{d\mathscr{E}_0}{dt}=-\frac{\mathscr{E}_0}{2T_{\rm cav}}-\frac{2i\omega}{\epsilon_0\pi w_0^2 L}\mathscr{P}+\frac{\mathscr{E}_t}{2T_{\rm cav}}e^{i\Delta\omega t}\,, \tag{15}$$

while the Bloch equations (1a) and (1b) are not changed.

As in the free-running maser case, we will solve these equations with the initial condition $\mathscr{E}_0=0$ and $\mathscr{P}\neq 0$, the initial value of $\mathscr{P}$ being given by the vacuum fluctuation description recalled above. The extra-source term in Eq. (15) accounts for the fact that, in the absence of any active medium ($\mathscr{P}=0$), the cavity would fill within a time $T_{\rm cav}$ with the triggering signal and the field inside the cavity would reach within this short time the steady state value $\mathscr{E}_0=\mathscr{E}_t e^{i\Delta\omega t}$. Equation (15) with the initial condition $\mathscr{E}_0(0)=0$ thus precisely describes the case of a triggering field which would be suddenly switched on at the cavity entrance mirror at the time of the maser pumping, and not the case of a continuous signal already present at time $t=0$ on the atoms, a situation more likely to occur. However, as $T_{\rm cav}$ is assumed to be much shorter than T_R, the cavity filling time is negligible compared to the maser evolution time and the two situations are equivalent. We thus can avoid to change the initial conditions of the problem, which would slightly complicate, without any benefit, the analysis to come. As we are in the fast-damping regime ($T_{\rm cav}<T_R$), the $d\mathscr{E}_0/dt$ term in Eq. (15) is negligible compared to $\mathscr{E}_0/2T_{\rm cav}$ and the Maxwell equation reduces to

$$\mathscr{E}_0=-\frac{4i\omega T_{\rm cav}}{\epsilon_0\pi w_0^2 L}\mathscr{P}+\mathscr{E}_t e^{i\Delta\omega t}\,, \tag{16}$$

which, combined to (1a) and (1b), describes the triggered maser evolution. We now proceed to solve these equations in the linear regime describing the early stage of the emission. $\mathscr{N}$ being close to N_0, one can replace $\mathscr{N}$ by N_0 in Eq. (1a) which becomes linear:

$$\frac{d\mathscr{P}}{dt}=\frac{id^2}{\hbar}\mathscr{E}_0 N_0\,. \tag{17}$$

Eliminating $\mathscr{E}_0$ between Eqs. (16) and (17), one gets

$$\frac{d\mathscr{P}}{dt}=\frac{\mathscr{P}}{2T_R}+\frac{d^2}{\hbar}N_0\mathscr{E}_t e^{i\Delta\omega t}\,. \tag{18}$$

To emphasize the similitude with Eq. (3b), we make the notation change,

$$\mathscr{P}=iN_0 d\theta_0 e^{i\phi}\quad(\theta_0 \text{ and } \phi \text{ real})\,, \tag{19}$$

and we get for $\theta_0\epsilon^{i\phi}$ the linearized evolution equation

$$\frac{d(\theta_0 e^{i\phi})}{dt}=\frac{\theta_0 e^{i\phi}}{2T_R}+\frac{\mathscr{E}_t d}{\hbar}e^{i\Delta\omega t}\,, \tag{20}$$

which can be deduced from Eq. (3b) by linearization (replacing $\sin\theta_0$ by θ_0) and by adding the triggering field term. We should note that, since the impinging field is assumed to be very small compared to the peak field of the maser emission, the triggering term in Eq. (20) should obviously satisfy the condition

$$\left|\frac{\mathscr{E}_t d}{\hbar}\right|\ll\frac{1}{T_R}\,. \tag{21}$$

Note also that, contrary to the case of Eq. (3a), the phase ϕ is now time varying: starting from the random phase ϕ_0^i, it can change in time to lock to the triggering field phase.

C. Solution of the linear regime: The triggering coefficient

Equation (20) shows that the complex Bloch angle evolution is due to two independent additive terms: the "spontaneous maser" term $\theta_0/2T_R$ and the triggering field contribution $(\mathscr{E}_t d/\hbar)e^{i(\Delta\omega t)}$. The solution of this equation with the initial condition $\theta_0(0)=\theta_0^i$ and $\phi(0)=\phi^i$ can be written as the sum of a spontaneous and a triggered term:

$$\theta_0(t)e^{i\phi(t)}=\theta_{\rm sp}(t)+\theta_{\rm trig}(t) \tag{22}$$

with

$$\theta_{\rm sp}(t)=e^{i\phi^i}\theta_0^i e^{t/2T_R}\,, \tag{23a}$$

$$\theta_{\rm trig}(t)=\theta_1(e^{t/2T_R}-e^{i\Delta\omega t})\,, \tag{23b}$$

$$\theta_1=\frac{\mathscr{E}_t d}{\hbar}\frac{1}{i\Delta\omega-(1/2T_R)}\,. \tag{24}$$

Note that in these equations, the quantities $\theta_{\rm sp}$, $\theta_{\rm trig}$, and θ_1 are complex quantities, contrary to θ_0, which remains a real angle. Let us now consider times t small enough for the linear regime to be still valid and large enough for $e^{t/2T_R}$ to be much bigger than $e^{i\Delta\omega t}$ in Eq. (23b):

$$T_R<t<T_R\ln N_0\,.$$

We can for such times neglect in Eq. (23b) the complex exponential and write

$$\theta_{\rm trig}(t)\simeq\theta_1 e^{t/2T_R}\,. \tag{25}$$

Equations (23a) and (25) now show that both the triggered and the spontaneous solutions increase exponentially at the same rate and stay proportional to each other. For the forthcoming discussion, it is convenient to introduce the absolute value of the ratio between the triggered amplitude and the average spontaneous solution:

$$\eta = \left| \frac{\theta_1}{\bar{\theta}} \right| . \tag{26}$$

η is a natural measure of the effect of the triggering which will be called the triggering coefficient.

From Eqs. (11) and (24), one gets

$$\eta^2 = \left| \frac{\theta_1}{\bar{\theta}} \right|^2 = \mathscr{L}\left(\Delta\omega, \frac{1}{2T_R}\right) \frac{\mathscr{E}_t^2 d^2}{\hbar} N_0 T_R^2 , \tag{27}$$

where

$$\mathscr{L}\left(\Delta\omega, \frac{1}{2T_R}\right) = \frac{\frac{1}{4T_R^2}}{\Delta\omega^2 + \frac{1}{4T_R^2}} . \tag{28}$$

$\mathscr{L}$ is the normalized Lorentzian function centered at the atomic frequency ($\Delta\omega = 0$), whose width is equal to the maser emission bandwidth.

Equation (27) can be given a simple physical interpretation in term of the number $n_{\text{cav}}^{\text{trig}}$ of triggering photons stored in the cavity. This number is defined by

$$n_{\text{cav}}^{\text{trig}} = \frac{\pi}{8} \frac{\epsilon_0 \mathscr{E}_t^2 L w_0^2}{\hbar\omega} . \tag{29}$$

We can thus eliminate $\mathscr{E}_t$ between Eqs. (27) and (29) and after some straightforward calculation taking into account Eqs. (4)–(7), one gets

$$\eta^2 = \mathscr{L}\left(\Delta\omega, \frac{1}{2T_R}\right) \frac{T_R}{T_{\text{cav}}} n_{\text{cav}}^{\text{trig}} . \tag{30}$$

In fact $(T_R/T_{\text{cav}}) n_{\text{cav}}^{\text{trig}}$ is nothing but the number of triggering photons impinging at the cavity entrance mirror during the time interval T_R. We will simply call $n_{\text{imp}}^{\text{trig}}$ this number:

$$n_{\text{imp}}^{\text{trig}} = \frac{T_R}{T_{\text{cav}}} n_{\text{cav}}^{\text{trig}} , \tag{31}$$

which allows us to write finally

$$\eta^2 = \mathscr{L}\left(\Delta\omega, \frac{1}{2T_R}\right) n_{\text{imp}}^{\text{trig}} \tag{32}$$

and even more simply, at resonance ($\Delta\omega = 0$),

$$\eta = (n_{\text{imp}}^{\text{trig}})^{1/2} . \tag{33}$$

Equation (33) merely states that the triggering coefficient is at resonance equal to the square root of the number of triggering photons impinging on the cavity during the maser characteristic evolution time.

D. Changes in maser emission delay and phase induced by the triggering field

Following the general procedure outlined in the introduction of this section, we now proceed to make the connection between the initial linear stage of the emission process and the subsequent nonlinear one. We choose arbitrarily to end the initial phase at a time t_0 such that, from this time on, the effect of the triggering field can be neglected. This condition can be expressed as

$$\frac{|\theta_0(t_0)|}{2T_R} \gg \left| \frac{\mathscr{E}_t d}{\hbar} \right| . \tag{34}$$

We want also $\theta_0(t_0)$ to be small enough for the linear regime to be valid up to time t_0, which can be expressed as

$$|\theta_0(t_0)| \ll 1 . \tag{35}$$

Equation (21) implies of course that conditions (34) and (35) are compatible and leaves some freedom for the definition of t_0 which must be taken of the order of a few T_R:

$$t_0 = qT_R , \tag{36}$$

q being of the order of a few units (smaller than $\ln N_0 \sim 10$).

For each choice of initial condition θ_0^i and ϕ^i, let us introduce the parameters θ^e and ψ^e defined as

$$\theta^e e^{i\psi^e} = e^{i\phi i} \theta_0^i + \theta_1 . \tag{37}$$

Then, according to Eqs. (22), (25), and (36), the linear solution of the evolution equation at time t_0 can be written as

$$e^{i\phi(t_0)} \theta_0(t_0) = \theta^e e^{i\psi^e} e^{q/2} . \tag{38}$$

This small value of the Bloch angle reached at time t_0 can now be considered as the new initial condition for the maser evolution during the nonlinear stage $t > t_0$. The evolution then obeys the nonlinear equation (3b) whose general solution is an hyperbolic secant pulse [Eq. (12)]. According to the

results of RAM I recalled in Sec. II A, we infer from that analysis that the maser pulse has the same shape as the free-running maser, with a phase ψ^e and a peak delay t_D such that

$$t_D - t_0 = -2T_R \ln\left[\frac{\theta^e e^{q/2}}{2}\right]$$

$$= -2T_R \ln\frac{\theta^e}{2} - qT_R \ . \tag{39}$$

The overall emission delay, measured from time $t=0$, is then

$$t_D = t_D - t_0 + qT_R = -2T_R \ln\frac{\theta^e}{2} \ . \tag{40}$$

Hence, as could have been expected, the maser characteristics (phase ψ^e and delay t_D) are independent of the arbitrary time t_0 chosen to perform the connection between the two emission phases. Equations (37) and (40), together with the probability laws (10a) and (10b) provide us with all the information needed to analyze the statistics of an ensemble of maser pulses triggered by the same field $\mathscr{E}_t e^{i\Delta\omega t}$. The maser pulses will somewhat fluctuate in phase and delay from one realization of the experiment to the next. These fluctuations are directly connected to the one of θ^e and ψ^e, which through Eq. (37) reflects those of the vacuum field. The magnitude of these fluctuations depends of course upon the size of the triggering coefficient η. The average values of the pulse delay and phase are also related to η. Instead of deriving cumbersome analytical formulas for these physical quantities, we can obtain them from simple geometrical arguments. The complex amplitude $\theta^e e^{i\psi^e}$ can be represented as a vector, sum of a "fluctuation-free" vector θ_1, and of a random one $\theta_0^i e^{i\phi^i}$, whose length is equal to θ_0^i and direction defined by ϕ^i. The tip of the $\theta_0^i e^{i\phi^i}$ vector is moving randomly from pulse to pulse without getting too far away from a circle of radius $\bar{\theta}=2/\sqrt{N_0}$. The construction of the $\theta^e e^{i\psi^e}$ vector is represented on Figs. 1(a) and 1(b) in the two cases $\eta<1$ and $\eta>1$. It is clear from this construction that the average value of θ^e is merely

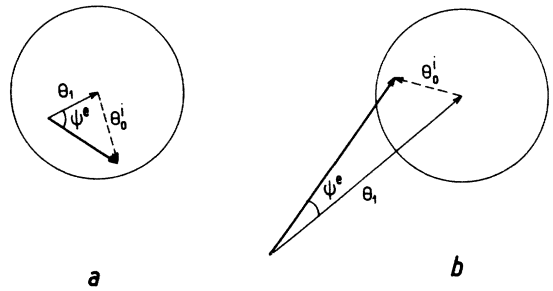

FIG. 1. Geometrical construction of the effective tipping angle parameters θ^e and ψ^e. The c number $\theta^e e^{i\psi^e}$ is represented by a vector, sum of the triggered contribution θ_1, and the spontaneous contribution θ_0^i. (a) Case of a small triggering coefficient $\eta<1$. (b) Case of a large triggering coefficient $\eta>1$.

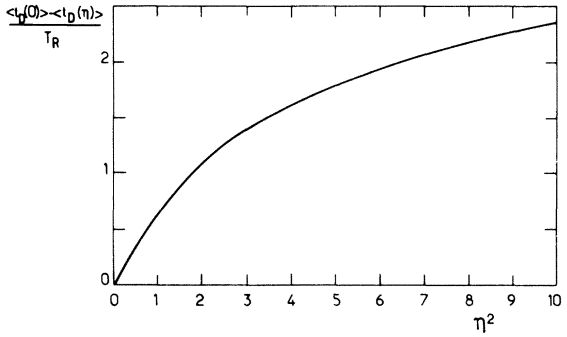

FIG. 2. Shortening $\langle t_D(0)\rangle - \langle t_D(\eta)\rangle$ of the maser emission delay versus the triggering coefficient η^2. Delay variation is measured in units of T_R.

$$\langle\theta^e\rangle = (\theta_1^2 + \langle\theta^2\rangle)^{1/2}$$

$$= \bar{\theta}(1+\eta^2)^{1/2} \ . \tag{41}$$

As a result the average delay of the triggered maser pulse is

$$\langle t_D(\eta)\rangle = T_R \ln\left[\frac{N_0}{1+\eta^2}\right] \ . \tag{42}$$

The variation of $\langle t_D(\eta)\rangle$ with η^2 is plotted on Fig. 2.

The delay fluctuation is directly linked to the length fluctuation of θ^e which the construction shows to be of the order of $\bar{\theta}$ (in both $\eta>1$ and $\eta<1$ cases). One thus has

$$\Delta t_D(\eta) = [\langle t_D^2\rangle - \langle t_D\rangle^2]^{1/2}$$

$$\sim 2\bar{\theta}T_R \frac{\partial}{\partial\theta^e}\ln\left[\frac{\theta^e}{2}\right]$$

$$= 2\frac{\bar{\theta}}{\langle\theta^e\rangle}T_R = \frac{2T_R}{(1+\eta^2)^{1/2}} \ .$$

This formula is of course only intended to give an order of magnitude. A more accurate expression should coincide with the free-running maser fluctuation when η is going to zero. One will thus take [see Eq. (13c)]

$$\Delta t_D(\eta) \simeq \frac{1.3 T_R}{(1+\eta^2)^{1/2}} . \tag{43}$$

The geometrical construction also shows that the average phase $\langle \psi \rangle$ is obviously the one of the impinging field. Taking this phase as a reference, we write

$$\langle \psi \rangle = 0 . \tag{44}$$

To estimate the order of magnitude of the phase fluctuations, we observe that the vector representing θ^e rotates randomly in all directions for $\eta < 1$ whereas it stays well defined in a finite angle when $\eta > 1$. We chose to call $\Delta\psi$ this angle and we thus get, after a mere inspection of Figs. 1(a) and 1(b),

$$\begin{aligned} &\Delta\psi \sim \pi \quad \text{for } \eta < 1 \\ &\Delta\psi \sim 2 \sin^{-1}\left[\frac{1}{\eta}\right] \quad \text{for } \eta > 1 . \end{aligned} \tag{45}$$

A more precise definition of the phase correlations which will be useful in the following is obtained by computing the average value $\langle \cos(\psi_i - \psi_j) \rangle$, where ψ_i and ψ_j are the phases of two independent maser pulses. This quantity is obviously going to zero for $\eta = 0$ [maximum phase fluctuations, large random values of the angle $\psi_i - \psi_j$, see Fig. 1(a)] and tending to 1 for $\eta \gg 1$ [small fluctuations; ψ_i and ψ_j are strongly correlated, see Fig. 1(b)]. The exact computation of this average involves some trigonometric calculations. One gets

$$\langle \cos(\psi_i - \psi_j) \rangle = f(\eta^2) \tag{46}$$

with $f(\eta^2)$ plotted on Fig. 3 (we will not give here the complicated analytical expression of this quantity).

Formulas (42) to (46), together with expression (32) giving η, describe all the effects of the triggering of a two-level atom maser by an external monochromatic field. The average delay and delay fluctuations are reduced by the triggering as well as the phase fluctuations. The change of the average delay is only logarithmic in η, whereas the reduction in phase and delay fluctuations is more sensitive (it involves more rapidly varying functions). The critical value above which the triggering effects become significant is $\eta = 1$. This value is achieved with a flux of one photon of resonant radiation impinging at the entrance mirror of the maser cavity during the characteristic maser time T_R. If the triggering field is detuned from resonance, the sensitivity to triggering decreases according to the Lorentzian law [Eq. (32)] and practically vanishes for a detuning of the order of the maser bandwidth $1/T_R$.

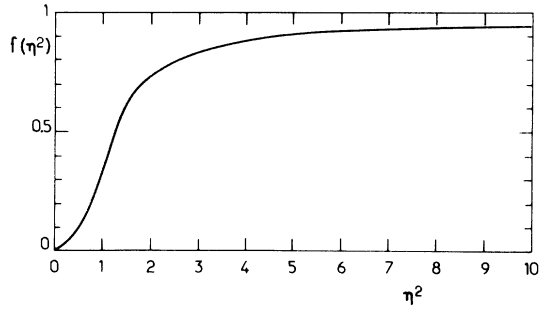

FIG. 3. Plot of the function $f(\eta^2)$ representing the variation versus η^2 of the maser emission phase correlation $f(\eta^2) = \langle \cos(\psi_i - \psi_j) \rangle$.

E. Polarization changes induced by the triggering field in a simple case

We now proceed to study the maser emission polarization changes induced by a linearly polarized triggering field. These effects are not described within the two-level atom model of previous subsections and require an analysis involving degenerate atomic transitions. The situation we have in mind is sketched in Fig. 4. The impinging radiation is polarized in a waveguide A and the output maser signal is analyzed in a waveguide B coupling the cavity to the detector. The A and B waveguides polarization directions are either parallel or perpendicular to each other. The atoms in the cavity oscillate

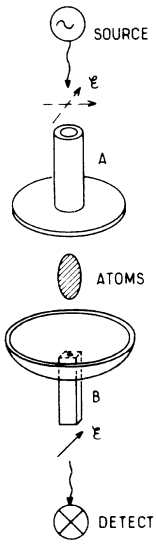

FIG. 4. General scheme of the setup allowing us to study the polarization-triggering effects.

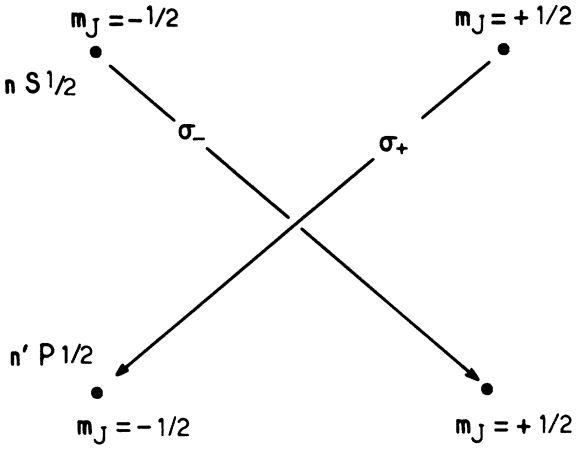

FIG. 5. Level scheme relevant to the $nS_{1/2} \rightarrow n'P_{1/2}$ maser emission.

on an $nS_{1/2} \rightarrow n'P_{1/2}$ transition, both levels having each a twofold degeneracy (see Fig. 5). Two circularly polarized field components $\mathscr{E}_0^+(t)$ and $\mathscr{E}_0^-(t)$ are emitted, respectively, along the

$$|nS_{1/2}, m_J = +1/2\rangle \rightarrow |n'P_{1/2}, m_J = -1/2\rangle$$

and

$$|nS_{1/2}, m_J = -1/2\rangle \rightarrow |n'P_{1/2}, m_J + 1/2\rangle$$

transitions (arrows in Fig. 5). When the maser is not triggered, these two components are radiated independently with uncorrelated phases and small random delay differences (as discussed in details in RAM I Sec. II J). The resulting field has then generally an elliptical polarization, almost linear for most of the pulse evolution time, with a big axis randomly rotating around the cavity axis from pulse to pulse. The detector accordingly "sees" signals strongly fluctuating from pulse to pulse, owing to the fact that the waveguide B projects along its fixed polarization direction this randomly oriented radiation.

If a linearly polarized field $\mathscr{E}_t e^{i\Delta\omega t}$ is impinging on the atoms, the two $\mathscr{E}^+(t)$ and $\mathscr{E}^-(t)$ field components are correlated to each other since they are both triggered by the projections $\mathscr{E}_t^+ e^{i\Delta\omega t}$ and $\mathscr{E}_t^- e^{i\Delta\omega t}$ of the same linearly polarized field along the two counterrotating polarization components (with a convenient phase choice, one has

$$\mathscr{E}_t^+ = \mathscr{E}_t^- = \mathscr{E}_t/\sqrt{2}$$

here). As a result the average phase and delay differences between $\mathscr{E}_0^+(t)$ and $\mathscr{E}_0^-(t)$ tend to decrease. The phases ψ^+ and ψ^- of the two circular components tend to lock to the common phase of the triggering field, which results in a locking of the maser polarization along the direction of the electric vector of the impinging radiation. More precisely, since $\mathscr{E}_0^{\pm} \sim e^{+i\psi_{\pm}}$, the averaged values of the radiated field intensities, respectively parallel and perpendicular to the triggering field, are

$$\begin{aligned} \langle |\mathscr{E}_{||}^2| \rangle &\propto 1 + \langle \cos(\psi_+ - \psi_-) \rangle , \\ \langle |\mathscr{E}_{\perp}|^2 \rangle &\propto 1 - \langle \cos(\psi_+ - \psi_-) \rangle , \end{aligned} \tag{47}$$

and the average polarization rate is

$$\begin{aligned} \mathscr{R} &= \frac{\langle |\mathscr{E}_{||}|^2 \rangle - \langle |\mathscr{E}_{\perp}|^2 \rangle}{\langle |\mathscr{E}_{||}|^2 \rangle + \langle |\mathscr{E}_{\perp}|^2 \rangle} \\ &= \langle \cos(\psi_+ - \psi_-) \rangle , \end{aligned} \tag{48}$$

where $\langle \cos(\psi_+ - \psi_-) \rangle$ is given by Eq. (46), η^2 being the triggering factor corresponding to one circular component of the impinging field. Hence, one can simply write

$$\mathscr{R} = f(\eta^2) , \tag{49}$$

which shows that the polarization rate varies exactly as the phase correlation function of the two-level atom maser. As soon as $\eta \gtrsim 1$, the maser emission becomes strongly polarized along the triggering field electric vector. This effect also results in a strong decrease of pulse to pulse fluctuations for the field transmitted by the analyzer to the detector. If B and A polarizations are parallel, one expects to get for $\eta \gg 1$ a nonfluctuating signal two times larger than the average free-running maser signal. If B and A polarizations are perpendicular, one predicts for $\eta \gg 1$ a near zero signal on the detector. These dramatic effects provide a very sensitive way of detecting the triggering field (see Sec. IV).

F. Triggering by blackbody radiation

The discussion of Sec. II E can easily be generalized to describe the effect of blackbody radiation triggering. In this case, however, the triggering field is incoherent and has a random phase and amplitude. Accordingly, the triggered contribution θ_1 to the Bloch angle is also a random quantity. Its fluctuation and average value are simply related to the Bose-Einstein statistics of the blackbody photon number. Let us call n_B the random number of blackbody photons which happen to be in the cavity mode at the time $t = 0$ when the maser is fired. The

probability $P(n_B)$ for the n_B distribution is given by the Boltzmann law:

$$P(n_B)=(1-e^{-1/\bar{n}_B})e^{-n_B/\bar{n}_B} \tag{50}$$

with an average value

$$\bar{n}_B=\left[\exp\left[\frac{\hbar\omega}{k_BT}\right]-1\right]^{-1}. \tag{51}$$

The frequency of these photons is distributed over the spectral width T_{cav}^{-1} of the maser cavity. According to Eq. (28), only the frequency components falling within the maser emission bandwidth $T_R^{-1}<T_{\text{cav}}^{-1}$ are effective for triggering the maser. As a result, the random number of blackbody photons to take into account is

$$n_B^{\text{trig}}=\frac{T_{\text{cav}}}{T_R}n_B \tag{52}$$

and the random blackbody triggering coefficient η_B is, according to Eq. (30),

$$\eta_B^2=\frac{T_R}{T_{\text{cav}}}n_B^{\text{trig}}=n_B\ . \tag{53}$$

η_B thus appears to be merely equal to the square root of the number of blackbody photons in the cavity mode. At the arbitrary time t_0 chosen to end the linear stage of the emission process, the maser Bloch angle is a random quantity given by Eq. (37) with random amplitude and phase parameter θ_B^e an ψ_B given by

$$\theta_B^e e^{i\psi_B}=e^{i\phi_i}\theta_0^i+e^{i\phi_B}\eta_B\bar{\theta}\ . \tag{54}$$

In this expression ϕ_i and ϕ_B are the random uncorrelated phases of the vacuum fluctuations and thermal radiation fields, respectively. θ_0^i is the random vacuum field amplitude obeying the Gaussian statistics of Eq. (10b) with a mean-square value $\bar{\theta}=2/\sqrt{N_0}$ and η_B is also, according to Eqs. (53), (50), and (51), a Gaussian quantity with a mean-square value $\eta_B=\bar{n}_B^{1/2}$. The sum of these two independent Gaussian parameters is again a random-phase Gaussian variable with a mean-square value equal to the sum of the mean-square values of its components:

$$\langle\theta_B^e\rangle^2=\bar{\theta}^2(1+\bar{n}_B)$$
$$=\frac{4}{N_0}(1+\bar{n}_B)\ . \tag{55}$$

Since the statistics of θ_B^e and θ_0^i obey the same general law, the behavior of the blackbody triggered maser pulses is described exactly by the same equations as the free-running ($T=0$) maser, provided one replaces in the expression of the initial Bloch angle N_0 by

$$N_0(1+\bar{n}_B)^{-1}\ .$$

The effect of the blackbody radiation triggering is thus to reduce the average delay to a new value

$$\langle t_D(T)\rangle=T_R\ln\left[\frac{N_0}{(1+\bar{n}_B)}\right] \tag{56}$$

without changing the phase and delay fluctuations. Of course, since the blackbody background is not polarized, the phases of the different polarization components of the maser emission are triggered by uncorrelated fields and the fluctuations of the polarization of the maser output are not affected by the blackbody photons. We thus establish theoretically all the results quoted without proof in RAM I.

G. External triggering of a maser at finite temperature

We end this section by discussing the case of practical interest in which a maser, triggered by blackbody radiation photons, is also subjected to a small fluctuationless external field. This situation is of course relevant to the problem of the noise of triggered maser detectors in which the signal to be measured is competing to initiate the system evolution not only with vacuum fluctuations but also with thermal radiation. During the early evolution phase of the emission, the two (thermal and external) fields add up their effects independently since the equations of motion are then linear. As a result, the Bloch angle at the end of this phase can be expressed as

$$\theta^e e^{i\psi_e}=\theta_B^e e^{i\psi_B}+\theta_1\ , \tag{57}$$

where θ_B^e and ψ_B are the random variables described in Sec. II F and θ_1 the triggered contribution computed in Sec. II D.

Equation (57) is strictly the same as Eq. (37) with the blackbody angles replacing the spontaneous ones. Since the statistics of these two random quantities obey the same law, the study of the subsequent maser evolution in this case strictly parallels the one we have developed in Sec. II D. We are led to define a temperature-dependent triggering factor as

$$\eta(T)=\left|\frac{\theta_1}{\langle\theta_B^e\rangle}\right|, \tag{58}$$

which according to Eq. (55) can be written as

$$\eta(T)=\left|\frac{\theta_1}{\bar{\theta}}\right|\frac{\bar{\theta}}{\langle\theta_B^e\rangle}$$
$$=\frac{\theta_1/\bar{\theta}}{(1+\bar{n}_B)^{1/2}}\ . \tag{59}$$

We recognize in this expression the triggering factor $\theta_1/\bar{\theta}$ corresponding to a $T=0$ K maser. Hence, all the effects of the triggering are described as in the $T=0$ K temperature case, provided one divide the triggering factor by $(1+\bar{n}_B)^{1/2}$. The new delay fluctuations, phase correlation, and polarization rates are still given by Eqs. (43), (46), and (49) with η being replaced by

$$\eta(T)=\left[\frac{\mathscr{L}\left[\Delta\omega,\frac{1}{2T_R}\right]n_{\rm imp}^{\rm trig}}{1+\bar{n}_B}\right]^{1/2}\ . \tag{60}$$

As for the average emission delay it is obtained from Eq. (42) by replacing N_0 by $N_0(T)$ and η by $\eta(T)$ and one gets the simple result

$$\langle t_D(T)\rangle=T_R\ln\left[\frac{N_0}{1+\bar{n}_B+\mathscr{L}n_{\rm imp}^{\rm trig}}\right], \tag{61}$$

which shows that the blackbody and external photons are adding their effects to shorten the emission delay.

The decrease with T of the effective triggering coefficient clearly describes the "noise" of the blackbody radiation background. The signal to be detected becomes unable to modify the maser properties as soon as $\eta(T)\lesssim 1$, i.e., as soon as the number of resonant photons impinging in the cavity per time interval T_R is smaller than the average blackbody photon number per mode.

III. GENERAL DESCRIPTION OF THE RYDBERG MASER TRIGGERING SETUP

We have described in details in RAM I the Rydberg maser system and the indirect detection procedure consisting in monitoring by field ionization the populations of the Rydberg levels involved in the maser transition. As already noticed, this method is not suited for the study of the time dependence of the maser emission since the atoms are analyzed after they have left the cavity, i.e., a long time after the emission has ended. Nor is it of course suited for a polarization or a phase analysis of the emitted radiation. In order to study these characteristics of the maser radiation, it is necessary to detect directly the microwave bursts of radiation. Using a Schottky diode heterodyne receiver, we have built such a detector and coupled it through a waveguide to the maser cavity. In this section we recall briefly for sake of completeness the main features of the Rydberg maser setup which have been described in detail in RAM I and we analyze more precisely the microwave apparatus used to trigger the maser and to detect the signals.

A. General view of apparatus

The general setup is outlined on Fig. 6. An open Fabry-Perot cavity is coupled by two waveguides to a tunable microwave source (Box 1) and to a millimeter-wave receiver [Boxes 2(a) and 2(b)]. The cavity is crossed by a Na atomic beam, excited by two collinear pulsed laser beams into the $33S_{1/2}$ Rydberg level (pulse repetition rate $\sim 5s^{-1}$). The cavity is tuned to resonance with the $33S_{1/2}\rightarrow 32P_{1/2}$, or $33S_{1/2}\rightarrow 32P_{3/2}$ transitions (107 892 MHz and 107 714 MHz, respectively) and the occurrence of maser action is checked by analyzing the atomic population level changes detected downstream the atomic beam by the field ionization detector (Box 3). Simultaneously, the bursts of mm wave are detected by the Schottky receiver and recorded by a fast transient digitizer scope interconnected to a videotape recorder and to a signal averager. The purpose of the experiment is to study the changes in delay, phase, and polarization induced by triggering the maser with a well-known small microwave field. We now proceed to describe in details the apparatus contained in Boxes 1 and 2 of Fig. 6.

B. Microwave triggering source (Box 1)

The very small amount of millimeter-wave radiation needed to trigger the maser pulses (typically in the pW range) is produced by frequency multiplying the output of an X band klystron in a homemade harmonic generator. The klystron is phase locked on a commercial quartz stabilizer (Microwave system MOS5) and its frequency is measured by a frequency counter. Its 100 mW microwave output around 12 GHz is sent through a 50 Ω coaxial cable to a Schottky diode mounted in a millimeter

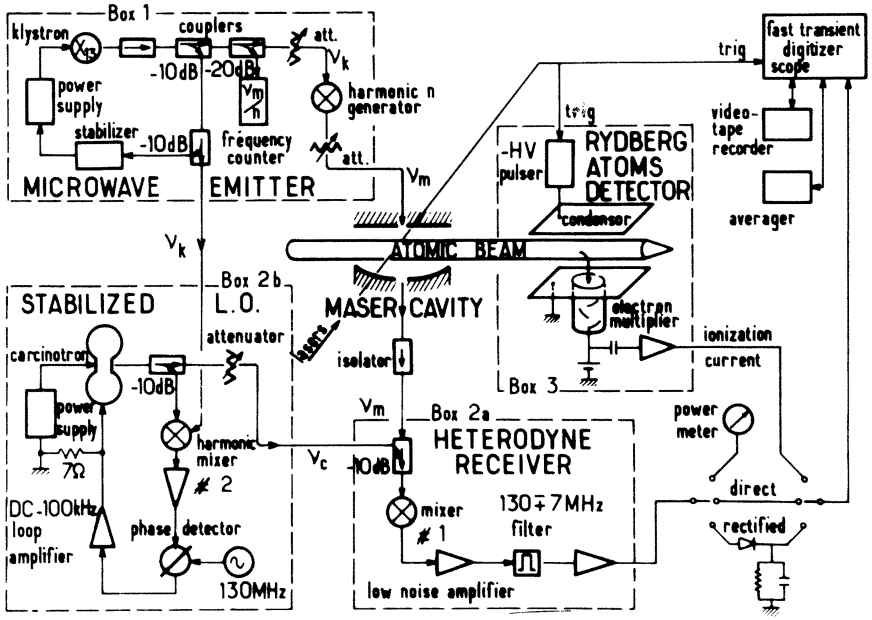

FIG. 6. General bloc diagram of the maser triggering experiment setup. Box 1: microwave triggering source system. Box 2(a): heterodyne receiver. Box 2(b): local oscillator providing the reference for the heterodyne receiver. Box 3: Rydberg atom field ionization detector for indirect detection of maser emission by population transfer monitoring.

waveguide and working as a frequency multiplier[7] (harmonic generator in Box 1). The working point of this diode is optimized by adjusting the direct bias current (0.5 to 20 mA) sent to the diode through a polarization tee. The inner dimensions of the diode waveguide mount are 2×1 mm^2 (F band) and the harmonic frequencies above the waveguide cutoff frequency (75 GHz) are generated. The following powers of harmonics are obtained: 100 μW at 84 GHz (harmonic rank $p=7$), 10 μW at 108 GHz, which is the frequency of interest ($p=9$), 1 μW at 180 GHz ($p=15$), and 10^{-7} W at 220 GHz ($p=18$). The $p=9$ harmonic is favored by tuning a back short mounted in the waveguide behind the diode. The cavity selection also helps reducing the power of other unwanted harmonics impinging on the atoms. Finally, the atoms resonant with the ninth harmonic are not at all sensitive to the very small amount of millimeter-wave power remaining at the other frequencies.

The power of millimeter-wave radiation impinging on the atoms is controlled by a variable 30-dB attenuator in front of the harmonic generator and by a second attenuator between the harmonic generator and the cavity. It can easily be reduced to the 10^{-12} W range and is estimated by measuring the power transmitted by the (empty) cavity and detected by the Schottky diode receiver (see below).

The frequency F of the triggering signal is directly obtained by measuring F/p with the frequency counter. It can be tuned by changing the klystron frequency. The spectral purity of this signal is better than a few kHz at 108 GHz, far below the $\sim$10 MHz bandwidth of the maser emission.

C. Millimeter-wave cavity and its coupling to the source and to the receiver

The triggering signal propagates first in a rectangular waveguide, and then is coupled through a rectangular-circular transition into a circular waveguide (brass pipe of 4-mm inner diam). By rotating the rectangular section of the guide around the circular guide axis, one can choose the linear polarization of the triggering signal impinging on the atoms. After the cavity, the outgoing signal is coupled to the detector by a rectangular guide which also plays the role of a polarization analyzer.

The coupling of radiation in and out the cavity is made through small (1.3-mm diameter) holes drilled in its mirrors. We have checked by using polarizing grids that the radiation polarization is not appreciably modified by passing through these coupling holes.

The cavity itself (cavity No. 1 of RAM I) is of

the Fabry-Perot semicofocal type. Its length L is connected to the resonant wavelength by the relation

$$L=\frac{\lambda}{8}(4q+1)\ . \tag{62}$$

In our case q is equal to 51 and the cavity lengths are $L_1=71.203$ and $L_2=71.321$ mm for the 107 892 and 107 714 MHz of the $33S\rightarrow 32P_{1/2}$ and $33S\rightarrow 32P_{3/2}$ transitions, respectively. The measured Q quality factor is 6100, yielding a characteristic decay time $T_{\rm cav}=9$ ns.

The coupling losses of the cavity are symmetrical. There is a 9.5-dB loss at the input mirror and another 9.5-dB loss at the output. These values have been estimated by measuring a total 19-dB loss for the cavity transmission and by checking that the millimeter-wave power needed to saturate an atomic transition inside the cavity is the same whether the millimeter wave is coupled through one mirror or the other. This loss figure means that the actual power impinging into the cavity is a factor $10^{0.95}\sim 9$ times larger than the power measured by the detector.

D. Millimeter-wave receiver

The detection is achieved by a Schottky diode heterodyne receiver mixing the signal to be measured with a reference millimeter wave produced by a stabilized carcinotron source. The detection setup is detailed in Boxes 2(a) and 2(b) of Fig. 6. The principle of the detector is to down convert the millimeter-wave frequency F to a low radio frequency value $F_{\rm rf}$ (equal to 130 MHz) by beating it in the mixing element shown in Box 2(a) (mixer No. 1) with a local oscillator frequency $F_{\rm LO}$ exactly 130 MHz apart from F. The mixing element is a GaAs Schottky diode originally built for radioastronomy.[8] The local oscillator [Box (2b)] is a Thomson-CSF carcinotron phase locked on the ninth harmonic of the X band klystron also used for generating the triggering signal (see Sec. III B above). The carcinotron stabilization procedure has already been described.[9] A small part of the klystron output (frequency F/p) is mixed to part of the carcinotron output in the harmonic mixer No. 2 [a Schottky diode of the same kind as the harmonic generator in Box No. 1 (Ref. 7)]. This mixer provides the pth harmonic of the klystron (frequency F) and beats it against the carcinotron output. The beat note is compared in a phase detector with the signal coming from a 130-MHz oscillator. The phase error signal is then converted into dc voltage, amplified, and added to the power supply voltage of the carcinotron in a standard feedback loop. As the klystron is exactly tuned to the frequency F/p, the carcinotron is automatically locked to the required frequency $F_{\rm LO}=F\pm F_{\rm rf}$.

The local oscillator signal is coupled to the receiver (harmonic mixer No. 1) through a directional 10-dB loss coupler. The receiver requires a local oscillator power of about 1 mW, so that a stabilized carcinotron power of ~ 10 mW is needed and easily obtained. The beat note generated at 130 MHz by the receiver is amplified in a wideband (0–250 MHz), low noise (1 dB), large gain (57 dB) preamplifier (Trontech W 110 F) followed by a 130 (± 7) MHz filter and by a 10–500 MHz, 20-dB gain final amplifier (SCD Nucletudes 5-20-2). The output beat note signal is then sent either to a powermeter for calibration, or directly fed into the fast transient digitizer scope, or else rectified by a diode so that an envelope signal proportional to the pulse intensity is produced and sent to the scope. The digitizer output is either directly recorded by a videotape recorder, allowing us to sample the successive pulses, or averaged and stored in a multichannel analyzer.

The noise characteristic figure of the detection chain is measured by coupling it to calibrated noise generators corresponding to various temperatures and measuring the changes in the dc background level on the powermeter. A noise temperature of 5000 ± 1000 K has been obtained, corresponding to a mm wave background power P_N of about 2.2×10^{-12} W in the 14 MHz $\times 2=28$ MHz double bandwidth of the detector.

Let us notice that it is very important in the maser triggering experiments to avoid a leaking of the local oscillator field back into the cavity. The carcinotron is indeed very powerful compared to the signals one wants to measure. To avoid these problems, a 35-dB isolator is inserted between the cavity and the receiver. The amount of carcinotron leaking signal into the cavity is then reduced to about 2 pW. This is still a signal whose magnitude is of the order of the triggering ones. However, it is 130 MHz apart from resonance and its effect on the maser operation is completely negligible.

IV. OBSERVATION OF THE MASER TRIGGERING SIGNALS

We now present the results of the triggering experiments performed with this setup. We start by a

brief description of the free-running untriggered maser signals.

A. Typical characteristics of the maser signals

Figure 7 shows two rectified maser emission pulses observed without external triggering on the $33S \rightarrow 32P_{1/2}$ transition of Na. The pulse to pulse intensity fluctuation are due in part to the randomness of the radiated polarization, but also to fluctuations in the initial conditions themselves (the masers are pumped by dye lasers whose power is not reproducible to better than $\pm 20\%$ from pulse to pulse).

Typically, the number of atoms involved in our masers is of the order of a few hundred thousand when they operate as shown in Fig. 7, well above threshold. This figure is obtained by direct field ionization measurement for pulses having typically the intensity shown in Fig. 7. Incidentally, this order of magnitude can also be confirmed by a simple time and amplitude analysis of these pulses. Average emission delays are about 300 ns with pulse duration of the order of 200 ns. A third of this duration (~ 80 ns) is due to the finite response time of the detection, so that one can estimate the real emission width as $T_W \sim 3.5 T_R \sim 120$ ns. This corresponds to maser characteristics emission times T_R of the order of 30 ns (note that T_{cav} is shorter, so that the masers are operating in the damped regime). Using formula (4) with $f = 120$, $\mu = 9.2 \times 10^{-3}$, and $\Gamma = 20\ s^{-1}$, one finds that the number of radiating atoms should typically be

$$N_0 \sim 6 \times 10^5 .$$

This figure is again confirmed by pulse intensity estimates. The detected maser peak power in Fig. 7 are about 15×10^{-12} W. The actually emitted power is about 20 times larger (there is a factor 9 coupling loss and an extra factor 2 because the field escapes the cavity at both ends). In a 200-ns time interval, we thus have 6×10^{-17} J of radiation corresponding to about 750 000 millimeter-wave photons, in fair agreement with the above estimate based on T_R measurements.

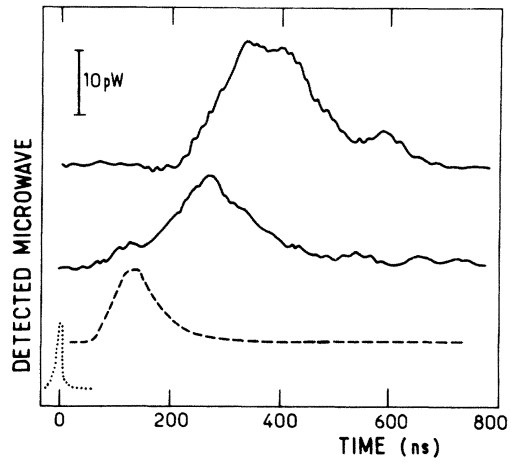

FIG. 7. Typical rectified maser pulse signals. Dotted-line curve represents the laser excitation. Dashed-line curve is the percussional response of the Schottky diode receiver. Two upper traces are typical maser signals obtained under identical conditions. Note the large pulse to pulse fluctuation. Number of emitting atoms is estimated to be $N_0 \sim 2 \times 10^5$.

B. Observation of delay, polarization, and phase changes induced by the triggering signals

When a small amount of millimeter-wave radiation is sent on the atoms with its electric field parallel to the detection waveguide polarization, one clearly observes a shortening of the emission delay and a strong decrease of the pulse to pulse amplitude fluctuations (Fig. 8). In order to quantitatively study these effects, we have averaged the free-running and triggered signal over 100 pulses (averaging time ~ 20 sec). Figure 9 exhibits typical triggering effects. Trace (a) corresponds to the averaged free-running maser output. Traces (b) and

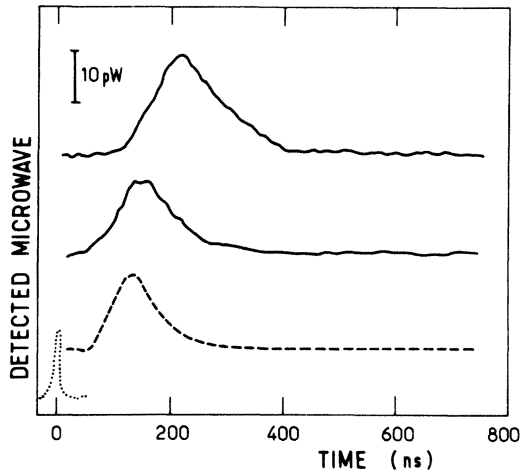

FIG. 8. Same signal as in Fig. 7 obtained with the addition of a $\sim 10^{-11}$ W triggering signal impinging on the atoms. Note the qualitative decrease in emission delay and fluctuation.

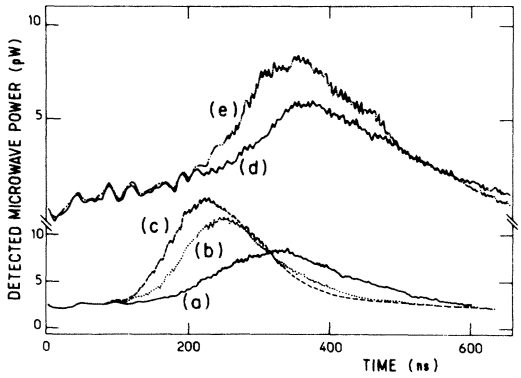

FIG. 9. Comparison between untriggered and triggered maser signals averaged over 100 pulses. Traces (a) and (d): untriggered masers; traces (b), (c), and (e) correspond to maser triggered, respectively, with 10^{-12}, 2.5×10^{-12}, and $\sim10^{-13}$ W.

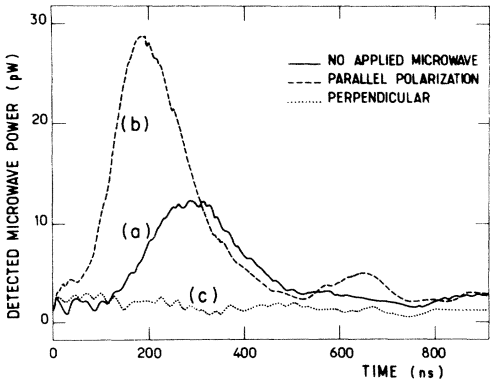

FIG. 10. Demonstration of polarization-triggering effects. (a) Untriggered maser signal averaged over a hundred pulses. (b) Maser triggered by a 10^{-11} W signal polarized parallel to the detector waveguide polarization vector. (c) Detector output corresponding to the same triggering power as in trace (b), the cavity being placed between crossed polarizer and analyzer.

(c) show the signals observed, for the same average pumping conditions, with a triggering power on the atoms of about 10^{-12} and 2.5×10^{-12} W, respectively. A still smaller triggering field effect is exhibited on traces (d) and (e): trace (d) shows again the free-running maser output and trace (e) a signal produced with a trigger power of only $\sim10^{-13}$ W. The reduction of the average emission delay is clearly apparent on these recordings. The intensity enhancement factor, i.e., the ratio $\langle I_t\rangle/\langle I_{sp}\rangle$ of the average triggered over spontaneous maser outputs is also very striking. This factor, which is related to the polarization rate of the maser radiation by the formula

$$\frac{\langle I_t\rangle}{\langle I_{sp}\rangle}=\mathscr{R}+1=1+f(\eta^2)\,, \tag{63}$$

tends to a maximum value equal to 2 for strong triggering fields. The polarized triggering field then channels all the maser energy in a well-defined polarization component and, on the average, twice as much energy is received by the detector. This effect is even more clearly displayed on Fig. 10 when we compare the free-running averaged maser signal [trace (a)] to the signal detected with an analyzer parallel to the triggering field [trace (b)] and to the signal detected with an analyzer perpendicular to that field [trace (c)]. In this last case, the maser energy is completely blocked by the analyzer. We have also qualitatively observed the predicted phase-correlation effect induced by the triggering. To perform this experiment, we take advantage of the fact that the low frequency 130-MHz signal used to lock the carcinotron is precisely at the frequency F_{rf} of the beat note produced by the Schottky receiver. This beat note contains the phase of the emitted radiation. By mixing it in a double balanced mixer with the low frequency signal serving as a fixed reference, one gets a voltage signal directly proportional to the cosine of the phase of the maser radiation. Averaging this signal amounts to measuring precisely the field correlation function studied in Sec. II D. Figure 11 shows a typical result. Trace (c) exhibits the phase correlation signal for a triggering field of 3×10^{-11} W. Traces (a) and (b) are test recordings showing that the correlation disappears when the triggering field is suppressed [trace (a)], or when it impinges on an empty cavity [trace (b)]. This effect is particularly

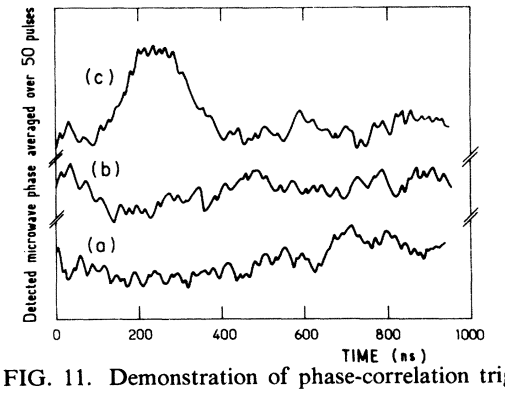

FIG. 11. Demonstration of phase-correlation triggering effects. Trace (a): phase correlation signal obtained with a 3×10^{-11} W triggering field. Trace (b): recording showing the diappearance of the signal when the Rydberg atoms are suppressed. Trace (c): recording showing the disappearance of the signal when the triggering field is suppressed (free-running maser).

convenient for field detection since it appears as a positive signal on a "black" background.

C. Data analysis; discussion of the sensitivity of the method for millimeter-wave signal detection

We have measured the polarization rates $\mathscr{R}$ and the delay variations corresponding to the signals registered in traces (b), (c), and (e) of Fig. 9, which were triggered with very small impinging fields. The obtained values for $\mathscr{R}$ and $\langle t_D(0)\rangle - \langle t_D(\eta)\rangle$ allow us to find with the help of Eqs. (42) and (46) triggering coefficients η^2 respectively equal to 23, 11, and 1. [Figures 12(a) and 12(b) show a fair agreement between the measured quantities and the theoretical predictions given by the solid lines.] This experiment can thus be considered as a measurement of very low levels of monochromatic radiation with a sensitivity of the order of the room temperature blackbody noise ($\eta^2=1$).

We have tried to check the consistency of these results with a direct measurement of the same impinging signals, transmitted to the heterodyne receiver through the cavity. In this control experiment, the maser was switched off (by suppressing the laser pumping), and the triggering signal transmitted by the cavity was measured by the powermeter connected to the Schottky receiver and to the amplifier chain. This measure amounts to comparing, on the logarithmic dial of the powermeter, the sum "noise + triggering signal" to the noise alone. An x dB increase above the noise level corresponds to a detected triggering power P_t such that

$$\log_{10}\frac{P_t+P_N}{P_N}=\frac{x}{10}\ , \tag{64}$$

or

$$P_t=P_N(10^{x/10}-1)\ . \tag{65}$$

The power impinging in the cavity, P_t^{imp}, is actually larger than P_t by a factor equal to the cavity to detector coupling losses (9.5 dB). Hence

$$P_t^{\text{imp}}=9P_N(10^{x/10}-1)\ , \tag{66}$$

P_t^{imp} can in turn be converted into a number of impinging photons per characteristic time T_R through the formula

$$n_{\text{imp}}^{\text{trig}}=\frac{P_t^{\text{imp}}\times T_R}{2\hbar\omega}\ . \tag{67}$$

(The factor 2 accounts for the fact that only one circular component of the impinging field actually triggers the maser pulses.) At last, using Eq. (60), it is possible to convert the $n_{\text{imp}}^{\text{trig}}$ values into triggering factors $\eta(T)$ (in our experiment $T=300$ K):

$$\eta^2(T)=\frac{9P_N(10^{x/10}-1)T_R}{2k_BT}\ . \tag{68}$$

It is clear that such a formula can yield only a very rough estimate for *absolute* values of $\eta^2(T)$, since the noise level [$P_N=2.2(\pm0.4)$ pW] is known with an uncertainty of $\pm20\%$, T_R is also estimated within $\pm20\%$ [$T_R=30(\pm7)$ ns], and the small-x fraction is measured within ±0.1 dB. For the impinging signals corresponding to traces (e), (b), and (c) of Fig. 9, one measures, respectively, $x=0.1(\pm0.1)$ dB; $x=0.2(\pm0.1)$ dB, and $x=0.5(\pm0.1)$ dB, corresponding to possible $\eta^2(T)$ values ranging between 0 and 15. A much more precise check is obtained by comparing the $\eta^2(T)$ values with each other, since the uncertainty on P_N and T_R then cancel out. The ratio between the number of triggering photons corresponding to traces (b) and (c) of Fig. 9 is found to be $2.5(\pm1)$, in fair agreement with the value $\frac{23}{11}$ given by the maser-triggering signals. Note that the smallest value ($\eta^2=1$) detected by the maser experiment could not be detected by the powermeter

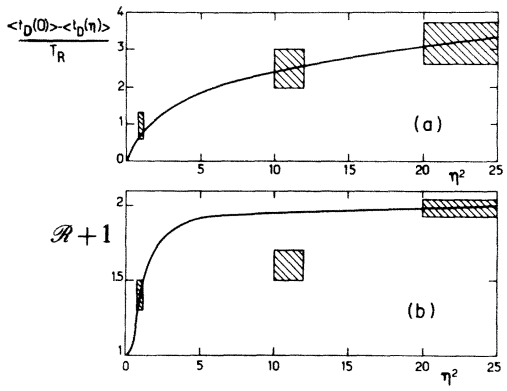

FIG. 12. Comparison between measured triggering effects (boxes) and theoretical predictions (solid-line curves). The three measured values correspond to the signals (c), (d), and (e) of Fig. 9. (a) Decrease of the maser emission delay. Theoretical curve is the same as in Fig. 2. (b) Increase of the maser polarization rate $\mathscr{R}+1$. Theoretical curve is deduced from the one in Fig. 3 by a vertical translation of 1 unit [see Eq. (63)]. In these figures, the vertical position of the experimental points are directly deduced from the maser signals (Fig. 9). The three horizontal positions (η^2 values) are obtained by a best fit to the theoretical curves, which can be considered as a measurement of the corresponding triggering signals. Note the fair agreement between experiments and theory, with only one point being 30% off the theoretical predictions.

[$x = 0.1(\pm 0.1)$ dB].

In conclusion, we may say that we have demonstrated the ability of these new types of millimeter-wave detectors to reach the thermal noise level at room temperature. An $\eta = 1$ signal corresponds to 10^{-13}W impinging on the atoms in a bandwidth of about 10 MHz, which expressed in detectivity is equal to 3×10^{-17} W/Hz$^{1/2}$. In principle, the quantum noise level should be reached when the cavity temperature is reduced to a value such that $k_B T \lesssim \hbar\omega$ ($T \lesssim 5$K at 100 GHz). A triggering factor of 1 would then correspond to a signal of 2×10^{-15} W and to a detectivity of $\sim 6 \times 10^{-19}$ W/Hz$^{1/2}$.

V. CONCLUSION AND PERSPECTIVES

Let us notice that the extreme sensitivity of these detectors to radiation is not intrinsic to the fact that the active medium is made of Rydberg atoms. Any super-radiant system working in this frequency domain would be as sensitive, even if the individual atomic dipoles were much smaller. The systems described in this paper are indeed reminiscent of cm-wave maser devices used as amplifiers in radioastronomy detectors.[10] (Let us note, though, that these masers were used in a cw amplifier mode and not in the transient regime described here.) The advantage of Rydberg-atom masers is that they can easily operate in the mm-submm-wave domain where they provide a very large number of potential resonant frequencies (see RAM I) with also the possibility of tuning over a wide frequency range the Rydberg lines by Stark effect.[11]

Another method for using Rydberg atoms as detectors has been recently proposed and demonstrated,[12] which makes use of the field ionization property of these atoms. In this method, the millimeter-waves photons are detected by the change in the Rydberg ionization current they produce when they are absorbed by an atom. This method also reaches the thermal noise level and blackbody radiation effects have been put in evidence in several Rydberg-atom experiments of this kind.[12–14] One should note that in these experiments the Rydberg atoms are sensitive only to the photon energy, whereas in our Rydberg maser experiments, we detect the field phase and polarization as well.

In order to improve the Rydberg maser detectors, several modifications of the experiment described in this paper appear to be called for. We have already mentioned the necessary reduction of the background temperature to about 5 K. Another improvement would be to replace the pulsed excitation by a cw laser pumping scheme. A small electric field acting periodically on the atoms would allow us to interrupt the continuous maser emission at a high repetition rate and to monitor how the oscillation is restored when this field is switched off. Repetition rates of 1 MHz are possible, i.e., an improvement of a factor 10^5 over the presently pulsed system. Changes in the transient behavior of these high repetition rate relaxing maser systems would allow us to measure with a much higher duty cycle small amounts of cw millimeter-wave triggering radiation, thus further increasing by time averaging the ultimate sensitivity of the system.

ACKNOWLEDGMENT

This work was supported in part by Direction des Recherches, Etudes, et Techniques Grant No. 80/187.

*Permanent address: Laboratore Fizica Atomica e Molecolare via del Giardino 3, 56100 Pisa, Italy.

[1] L. Moi, P. Goy, M. Gross, J. M. Raimond, C. Fabre, and S. Haroche, Phys. Rev. A 26, xxx (1982).

[2] Q. Vrehen and M. Schuurmans, Phys. Rev. Lett. 42, 224 (1979).

[3] N. W. Carlson, D. J. Jackson, A. L. Schawlow, M. Gross, and S. Haroche, Opt. Commun. 32, 350 (1980).

[4] M. Gross, thesis, University of Paris VI, 1980 (unpublished); M. Gross and S. Haroche, Phys. Rep. (in press).

[5] F. Haake, H. King, G. Schroder, J. Hauss, and R. Glauber, Phys. Rev. A 20, 2047 (1979).

[6] D. Polder, M. Schuurmans, and Q. Vrehen, Phys. Rev. A 19, 1192 (1979).

[7] P. Goy, J. Int. Infrared Millimeter Waves 3, 221 (1982).

[8] L. Moi, C. Fabre, P. Goy, M. Gross, S. Haroche, P. Encrenaz, G. Beaudin, and B. Lazareff, Opt. Commun. 33, 47 (1980).

[9] P. Goy, C. Fabre, M. Gross, and S. Haroche, J. Phys. B 13, L-83 (1980).

[10] See, for example, A. E. Siegman, *Microwave Solid-State Masers* (McGraw-Hill, New York, 1964).

[11] T. Ducas, W. Spencer, A. Vaidyanathan, W. Hamilton, and D. Kleppner, Appl. Phys. Lett. 35, 382 (1979).

[12] H. Figger, G. Leuchs, R. Straubinger, and H. Walther, Opt. Commun. 33, 37 (1980).

[13] P. Koch, H. Juronymus, A. Van Roan, and W. Raith, Phys. Lett. 75A, 273 (1980).

[14] W. Spencer, A. Vaidyanathan, T. Ducas, and D. Kleppner, Phys. Rev. A 24, 2513 (1981).